Structural, dielectric and electrical studies of $MgAl_{2-2x}Y_{2x}O_4$ (x=0.00–0.05) cubic spinel nano aluminate

Rohan Samkaria · Vimal Sharma

Abstract Investigations were carried out on a series of $MgAl_{2-2x}Y_{2x}O_4$ (x=0.00–0.05) nanoparticles prepared in steps of 0.01 by chemical co-precipitation method to study the effect of yttrium substitution at aluminum site on the structural, dielectirc and electrical properties. The single phase cubic spinel structure of all the samples was confirmed by X-ray diffraction (XRD). The Fourier transform infrared spectroscopy (FTIR) study shows two strong absorption bands in the frequency range 400–800 cm^{-1}, on the tetrahedral and octahedral sites respectively. Elemental analysis by Energy dispersive X-ray fluorescence (EDXRF) shows that samples are stoichiometric. The scanning electron microscopy (SEM) study reveals surface morphology of nanoparticles. Transmission electron microscopy (TEM) study shows the individual nanoparticles size and validates the nanocrystalline nature of the samples. The variation of dielectric permittivity at room temperature as a function of frequency (1 KHz to 1 MHz) suggests the dielectric dispersion due to Maxwell-Wagner Interfacial Polarization. AC conductivity study reveals that the conduction is due to small polaron hopping. The electrical modulus analysis shows that nanocrystalline $MgAl_{2-2x}Y_{2x}O_4$ system exhibits non Debye type relaxation. The dc resistivity was found to increase with increase in yttrium content.

Keywords Ceramics · Nanocrystalline materials · X-ray diffraction · Transmission electron microscopy · Dielectric response

R. Samkaria · V. Sharma (✉)
Department of Physics, National Institute of Technology Hamirpur, Hamirpur 177005, India
e-mail: vml16sharma@yahoo.co.in

R. Samkaria
e-mail: rohan.samkaria@gmail.com

1 Introduction

Spinel oxides which has general formula AB_2O_4, where A and B are the divalent and trivalent cations respectively, have received interest due to their structural features which facilitate tailoring of various properties [1]. They provide technical applications, such as an industrial refractory material, in chemical catalysis, electronics industry and integrated circuit technology [2]. Among these materials, aluminum based Magnesium aluminate spinel ($MgAl_2O_4$) has received attention because of its excellent physical properties such as high melting point, high mechanical strength at elevated temperatures, resistance to radiation damage, low permittivity and low loss tangent. Due to which it has demonstrated potential use for variety of applications such as an industrial refractory material and as a tunable dielectric material for microwave devices [3, 4].

With the advent of nanotechnology the current research activities on $MgAl_2O_4$ spinel mainly focuses on the improvement of properties through the introduction of suitable dopant and synthesis technique, by reducing dimensions down to the nanoscale. This is primarily because in nanocrystalline materials the physical properties are controlled more by the grain boundaries than by the grains [5, 6].

The nature of ionic bonding dominates in $MgAl_2O_4$ spinel due to which it has high electrical resistivity, thereby classifying this material as a dielectric. An understanding of the dielectric properties of nanosized $MgAl_2O_4$ in terms of particle size, temperature, and frequency of the applied field was developed by Kurien. He explored that the material can be considered to prepare dielectric components in microwave integrated circuits [7]. Moreover in order to optimize the dielectric properties there are several reports in literature expressing the doping effect of various

metal cations in $MgAl_2O_4$. These reports suggest that the trivalent aluminum cation at octahedral sites greatly determine the polarization in spinel aluminates and better optimization of electrical properties were achieved when divalent and trivalent cations of transition metals are subsituted at the tetrahedral and octahedral sites respectively [8–11].

Recent studies has reported that replacements of Fe^{3+} with suitable rare earth ions in spinel ferrites strongly influence the electrical transport properties of subsituted samples, thereby making them more superior for high frequency applications [12, 13], owing to similarity between the polarization and conduction mechanism in spinel ferrites and aluminates. A rich behaviour can also emerge out in the electrical transport properties of spinel aluminates with rare earth substitution at the octahedral B site.

However to best of our knowledge there was no comprehensive study is available in literature related to the effect of rare earth substitution on the dielectric and electrical properties of nanosized spinel aluminates; this article fulfills that gap. The chemical coprecipitation technique is used for the preparation of samples. This method yields the composition of prepared samples close to that of stoichiometric spinel when prepared in more basic conditions and this idea motivates the authors to prepare their samples at pH 10 [14].

In the present study Y^{3+} doped single phase composition of $MgAl_2O_4$ are prepared, and the structural and electrical properties are investigated systematically.

2 Materials and methods

2.1 Materials used

All the compositions of $MgAl_{2-2x}Y_{2x}O_4$ (x=0.00–0.05) series were prepared from Merck Germany GR grade chemicals viz. $Mg (NO_3)_2.6H_2O$, $Al (NO_3)_3.9H_2O$, $Y (NO_3)_3.9H_2O$ and aqueous NH_3 (Merck India, 30 %). The chemical co-precipitation technique was used to synthesize the samples described elsewhere [9]. Basically this technique involves a physical chemical process in which soluble metals and inorganics were converted to relatively insoluble metal and inorganic salts by the addition of an alkaline reagent which raises the solution pH to lower the solubility of the metallic constituents and thus bring about precipitation.

2.2 Methods of characterization

The X-ray diffraction pattern of the powder samples were recorded with a Panalytical 3050/60 Xpert-PRO using Cu K_α radiation. The FTIR spectrum was recorded in the IR region from 400 to 800 cm^{-1} by Perkin Elmer Spectrum-65. Energy dispersive X-ray fluorescence was used to determine the chemical composition of the compounds using Panalytical

Epsilon-5. The microstructure of the samples was studied using scanning electron microscopy ZEISS EVO 40. Particle sizes were analyzed by means of Transmission electron microscope JEOL JEM 2100F operated at 200 kV. For dielectric measurements nanoparticle powder was consolidated in the form of pellets of 13 mm diameter and thickness of 1 mm. The pellets were polished with silver paste to provide electrode contacts. The room temperature dielectric properties as a function of frequency were measured from 1 kHz–1 MHz using Wayne Kerr 6500B Impedance Analyzer. The DC electrical resistivity was measured using Electrometer (Keithley, Model 6517A) in the temperature range of 303–373 K by two probe method.

3 Results and discussion

3.1 Structural properties of $MgAl_{2-2x}Y_{2x}O_4$ (x=0.00–0.05) system

The X-ray diffraction pattern of $MgAl_{2-2x}Y_{2x}O_4$ ($0.00 \leq x \leq 0.05$) system show good crystallization with well defined diffraction lines Fig. 1. The diffraction peaks with Miller indices (111), (220), (311), (400), (511) and (440) correspond to the spinel structure of $MgAl_2O_4$ (JCPDS Card No. 21–1152). The absence of any extra peak in these patterns indicates the formation of single phase cubic spinel structure. The lattice constant (a) was determined from the most intense peak (311) using the relation [15]:

$$a = d\left[\left(h^2 + k^2 + l^2\right)\right]^{\frac{1}{2}}, \quad (1)$$

where h, k, l are the miller indices and d is the value of interplannar spacing. The unit cell volume was calculated
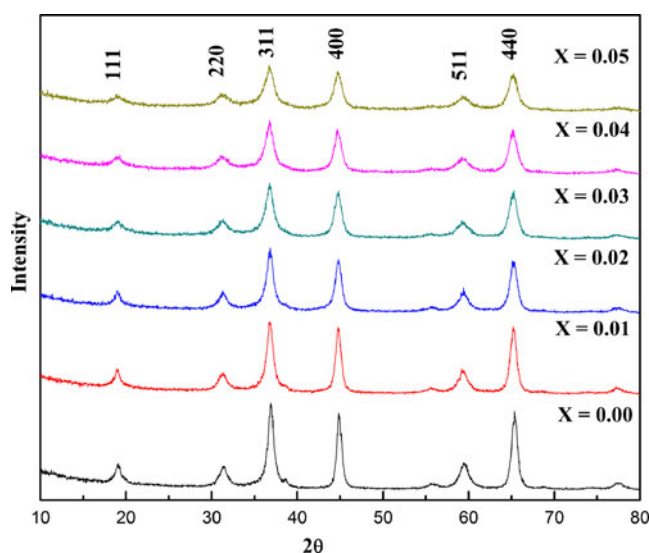
Fig. 1 X-ray diffraction pattern for the $MgAl_{2-2x}Y_{2x}O_4$ (x=0.00–0.05) system

using $V_{cell} = a^3$. The crystallite size (D) was determined from the most intense peak (311) using Scherrer formula [15]:

$$D = \frac{k\lambda}{\beta \cos\theta},$$ (2)

where β is the full width at half maximum of the peak after correcting for peak broadening caused by the diffractometer, λ is the X-ray wavelength (1.5418 Å), θ the Bragg's angle and k depends on unit cell geometry, having value equal to 0.9 for cubic structure. The X-ray density (d_{x-ray}) was determined from the volume of a single unit cell using the relation [15]:

$$d_{x-ray} = \frac{ZM}{V_{cell} N_A},$$ (3)

where Z is the number of formula units per unit cell ($Z = 8$ for cubic spinel), M the molar mass, V_{cell} volume of the unit cell and N_A is the Avogadro's number. It is observed from Fig. 2 that the lattice constant and X-ray density increases with increase in yttrium content for all compositions. This increase in lattice constant is due to the replacement of smaller Al^{3+} ions (0.53 Å) with larger Y^{3+} ions (0.90 Å) which causes dilation of the spinel lattice and results in the increase of lattice constant. The increase in X-ray density of all the samples is due to the higher atomic mass of Yttrium (88.906) than that of Aluminum (26.982) [16].

The variation of crystallite size at different 'x' values is given in Table 1. It can be seen that the Crystallite size decreases with increase in yttrium content. A possible reason for such a trend of crystallite size on concentration is that, the crystallite growth depends on grain boundary mobility and increasing yttrium concentration reduces the grain growth due to segregation on or near the grain boundaries which hampers the grain boundary movement thereby decreasing the crystallite size [14].
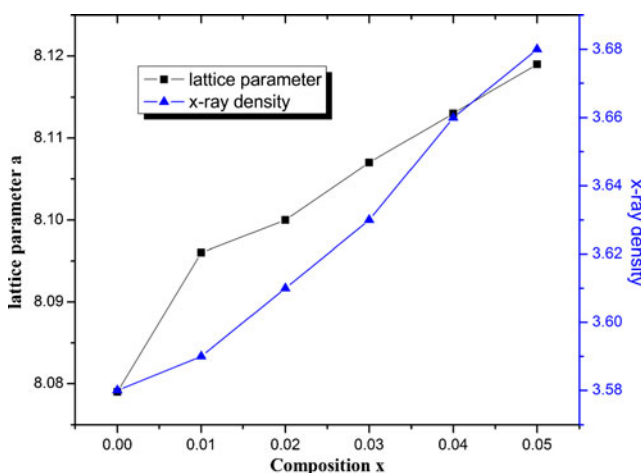
The FTIR spectra for all the samples are shown in Fig. 3. Band position in FTIR spectra for spinel $MgAl_2O_4$ depends on Al^{3+}-O^{2-} distances for the tetrahedral and octahedral complexes. Absorption bands around 700 cm^{-1} (ν_1) and 530 cm^{-1} (ν_2) are attributed to the stretching vibrations of Al-O in tetrahedral and octahedral coordination states respectively and hence confirming the formation of spinel structure [17]. In addition the study also predicted that with addition of yttrium the intensity of absorption band at (ν_1) remains nearly constant whereas the intensity of absorption band at (ν_2) is suppressed. This decrease in intensity of band ν_2 is attributed to the to the occupancy of yttrium ions on octahedral (B) sites, which due to their larger ionic radius than aluminum ions affect the Al^{3+}- O^{2-} distance at the octahedral sites. Consequently the system goes into a more disordered state; hence less intense bands in FTIR spectra are observed [18].

The chemical composition of the samples determined using Energy dispersive X-ray fluorescence technique is shown in Table 1. The results confirm that the theoretical molar ratios and the experimentally calculated molar concentration of the different elements present are in good agreement with each other. Also it can be inferred, that Y^{3+} ions are replacing Al^{3+} in the FCC unit cell of magnesium aluminate at the octahedral site meeting 1: 2 divalent to trivalent ratio. A scanning electron microscopic (SEM) image for the samples ($x = 0.00$, 0.05) is shown in Fig. 4. Surface morphology of the samples indicates the agglomeration of crystallites to form large particles. Figure 5 shows the transmission electron microscope (TEM) image of the pure and doped ($x = 0.05$) samples. From this figure, it is observed that the particle size lies in nano regime and is larger than the crystallite size calculated from the XRD data, which suggests that the nanoparticles are formed due to aggregation of different crystallites. The selected area electron diffraction pattern (SAED) of the samples ($x = 0.00$, 0.05) is shown in Fig. 6. The figure demonstrates the polycrystalline nature of the compounds and is indexed to the cubic spinel structure of the nanoparticles.

3.2 Dielectric response

3.2.1 Compositional and frequency dependence of dielectric constant

The dependence of dielectric constant (ε') on composition in the frequency range from 1 kHz to 1 MHz is shown in Fig. 7. Form this figure; it is clear that the dielectric constant decreases with increase in yttrium content. This type of behavior can be explained due to the formation of ordered spinel phase in all the samples [19, 20], and by the suppositions suggested by Rezlescu and Iwauchi [21, 22]. They reported that for spinel compounds the mechanism of

Fig. 2 Variation of lattice constant (a) and X-ray density (dx-ray) for the $MgAl_{2-2x}Y_{2x}O_4$ ($x = 0.00$–0.05) system

Table 1 Structural and electrical parameters for the MgAl2-2xY2xO4 (*x*=0.00–0.05) system

Parameters	MgAl$_{2-2x}$Y$_{2x}$O$_4$					
	0.00	0.01	0.02	0.03	0.04	0.05
Lattice Parameter, a (Å)	8.079	8.096	8.100	8.107	8.113	8.119
Cell Volume, V cell (Å^3)	527.3	530.6	531.4	532.8	534.0	535.2
X-ray Density, $d_{x\text{-ray}}$ (g cm^{-1})	3.58	3.59	3.61	3.63	3.66	3.68
Crystallite Size, D (nm)	10.27	8.95	8.32	7.11	7.05	6.25
Polaron radius, r_p (Å)	0.710	0.712	0.713	0.713	0.714	0.715
Jump Length, L (Å)	2.856	2.862	2.863	2.866	2.868	2.870
Dielectric constant, ε' (1 MHz)	7.35	6.89	6.68	6.57	6.54	6.02
Loss tangent, $tan\delta$ (1 MHz)	0.1430	0.1201	0.1185	0.0999	0.0786	0.0734
AC conductivity, $\sigma_{a.c.}\times10^{-5}$ (1 MHz)	5.88	4.67	4.36	3.71	2.88	2.51
Resistivity, ρ (Ω cm)$\times10^9$ (303 K)	1.26	1.58	1.92	2.82	3.61	5.16
Mg (mol) ±5 %	1.03	1.06	1.04	0.97	0.94	1.01
Al (mol) ±5 %	2.00	1.94	1.92	1.91	1.87	1.77
Y (mol) ±5 %	–	0.001	0.024	0.036	0.043	0.062
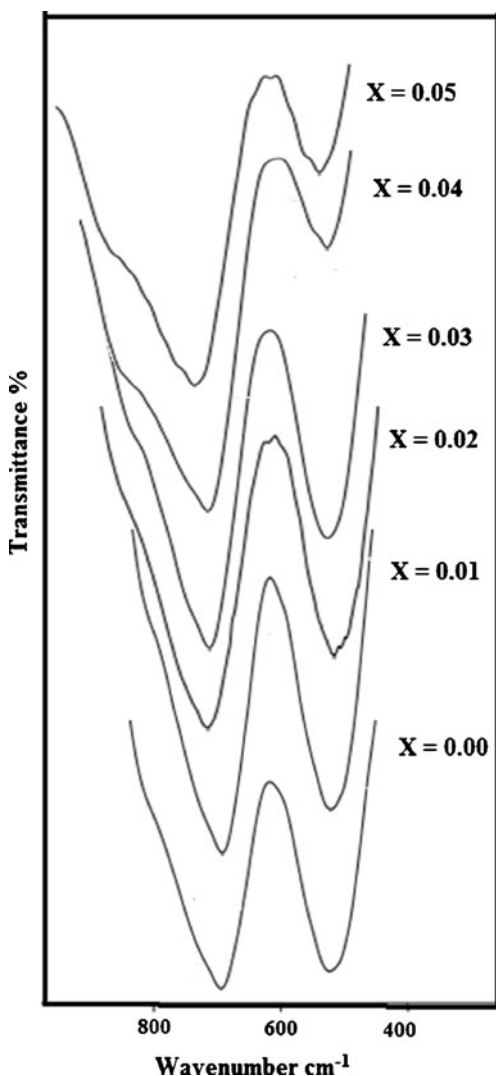
Fig. 3 FTIR pattern for the MgAl$_{2-2x}$Y$_{2x}$O$_4$ (*x*=0.00–0.05) system

electrical conduction is similar to that of the dielectric polarization. For the present system MgAl$_{2-2x}$Y$_{2x}$O$_4$ (0.00≤ x≤0.05) the electrons exchange between Al^{3+} and Al^{2+} ions gives local displacement of electrons in the direction of an applied electric field as a result of which polarization is induced. Now it can be seen from Table 1 that the molar concentration of aluminum decreases continuously with increase in yttrium concentration. Therefore due to depletion in the concentration of Al^{3+} ions, the electron transfer between Al^{2+} ↔ Al^{3+} will be hindered as a consequence of which the net polarization will decrease and hence dielectric constant decreases with increase in yttrium content.

Dielectric constant for all the samples showed dispersion with frequency Fig. 7. This behaviour of the dielectric constant as a function of frequency can be explained by Maxwell–Wagner type interfacial polarization in accordance with Koops phenomenological theory [23, 24]. Koops suggested a theory in which the samples having heterogeneous structure contain well conducting grains separated by highly resistive thin grain boundaries. In the present study solid samples in the form of pellets are imagined to consist of well conducting grains separated by poorly conducting grain boundaries, thereby creating inhomogeneities which give rise to a frequency dependent polarization. Now with the application of external applied field the charge carriers accumulate at the less conducting grain boundaries thereby creating interfacial polarization. At lower frequencies these charge carriers can follow the external applied field alternations thereby contributing to the interfacial polarization, whereas at higher frequencies the electron exchange between charge carriers cannot follow the external alternating field, due to which there is decrease in contribution towards interfacial polarization resulting in low dielectric constant at higher frequencies.

Fig. 4 SEM images of $MgAl_{2-2x}Y_{2x}O_4$ (**a**) $x=0.00$, (**b**) $x=0.05$
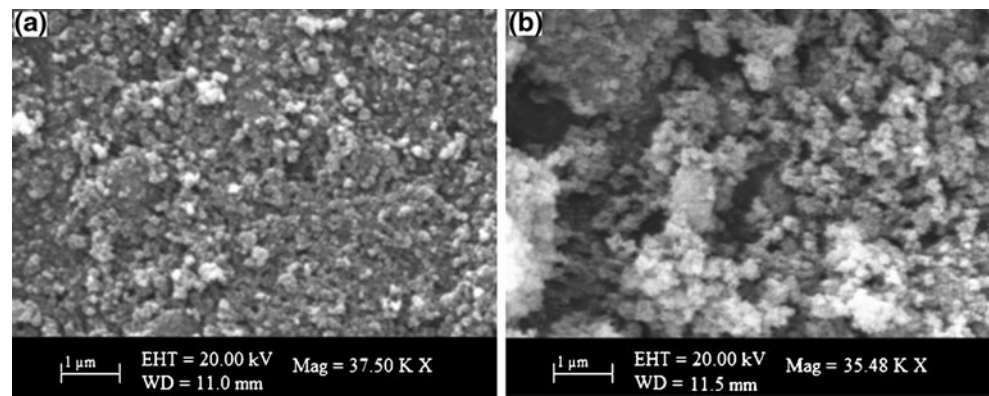
3.2.2 Compositional and frequency dependence of dielectric loss tangent

It is clear from Fig. 8 that loss tangent (*tanδ*) decreases with an increase in yttrium concentration for $MgAl_{2-2x}Y_{2x}O_4$ series. A decrease in Al^{3+}/Al^{2+} pairs available for conduction with an increase in yttrium concentration at the octahedral site is considered to be responsible for this type of behaviour. It can also be seen from Fig. 8 that *tanδ* decreases with increase in frequency for all samples. This behaviour can be explained in the basis of domain wall resonance. At lower frequencies more energy is required for polarization in the grain boundaries due to which energy loss is high on the other hand at high frequency polarization between grain boundaries is inhibited due to which the value of *tanδ* is found to be low at higher frequencies.

3.2.3 AC conductivity studies

In spinel $MgAl_2O_4$ the charge carriers are not free but are strongly localized. Therefore conduction occurs by the hopping of charge carriers between these localized states, this localization may be due to the formation of polarons. In small polaron hopping the distortion of the lattice induced around a charge carrier, extends over distances smaller than the lattice parameter. Hence in order to determine the type of polarons responsible for conduction mechanism, the polaron radius (r_P) is calculated for all the samples by the relation [25]:

$$r_p = \frac{1}{2}\left[\frac{\pi}{6N'}\right]^{\frac{1}{3}}, \qquad (4)$$

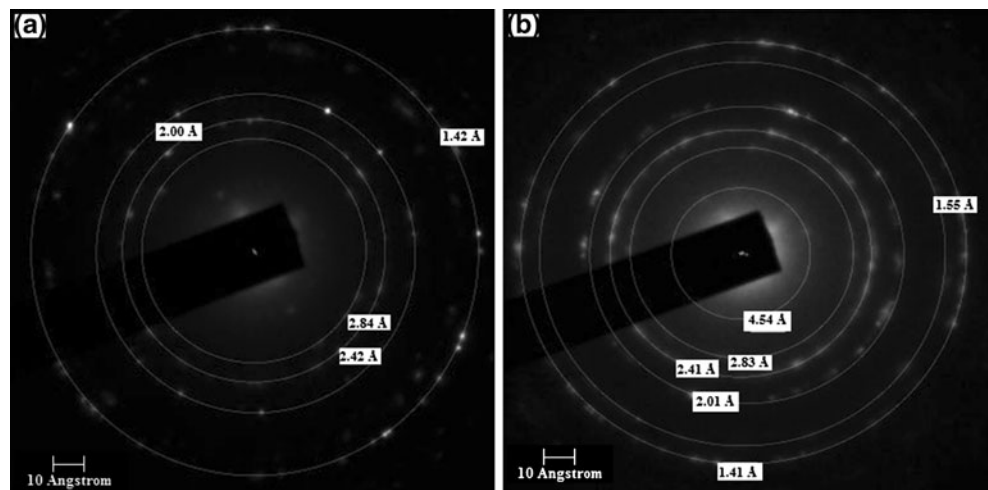where N' is the number of sites per unit volume = $96/a^3$.

Calculated values of polaron radius are summarized in Table 1. The values are found to be smaller than the lattice parameter (*a*). Therefore the calculated values of polaron radius suggest the presence of small polarons type charge carriers in all the investigated samples.

The variation of ac conductivity ($\sigma_{a.c.}$) as a function of frequency is represented in Fig. 9. From which it is clear that ac conductivity increases with increase in frequency. This can be explained by the fact that, as frequency of the applied field increases, the conductive grains become more active, thereby promoting transition between Al^{3+} and Al^{2+} ions at octahedral sites in the spinel lattice, due to which the hopping conduction increases with frequency. Also the electrical conduction mechanism in terms of polaron hopping model was discussed by Austin and Mott [26]. They have suggested that in large polaron hopping the ac conductivity decreases with frequency whereas in small polaron hopping it increases with frequency. Consequently from the plots of ac conductivity we can say that the conduction mechanism for all the samples occurs due to formation of small polaron type charge carriers among the localized states.

Fig. 5 TEM images of $MgAl_{2-2x}Y_{2x}O_4$ (**a**) $x=0.00$, (**b**) $x=0.05$
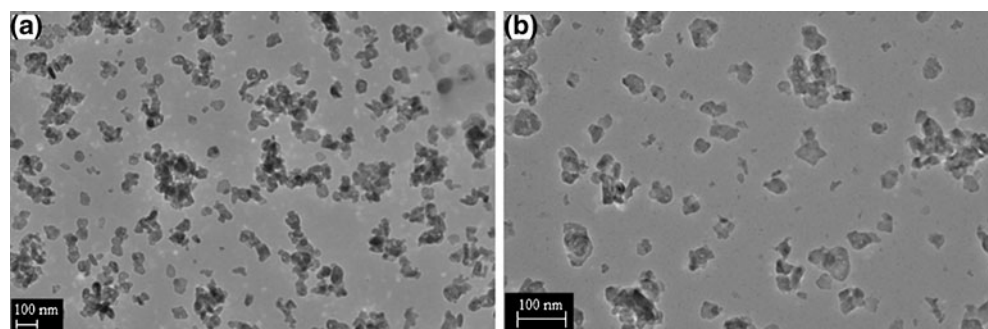
Fig. 6 Selected area electron diffraction pattern (SAED) showing the characteristic crystal planes of MgAl$_2$$_{-2x}Y_{2x}O_4$ (a) x=0.00, (b) x= 0.05
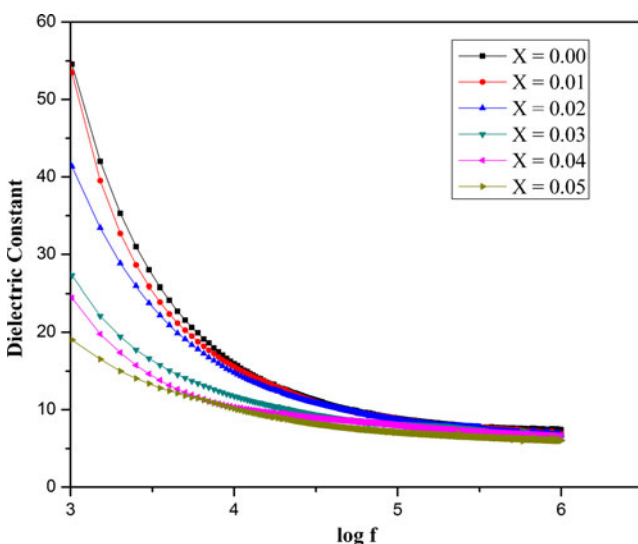

3.2.4 Electrical modulus studies

In recent years electrical relaxation in ionically conducting materials has been extensively studied and analyzed in terms of modulus formalism. The advantage of representing the electrical relaxation in modulus formalism is that the electrode polarization effects are suppressed in this representation. This happens because of the insensitiveness of the frequency dependence of the imaginary part of the modulus M'' to the polarization processes, provided these were characterized by capacitances which are much larger than the bulk capacitance [27].

The dielectric modulus is derived from the inverse of the complex dielectric constant ε^*.

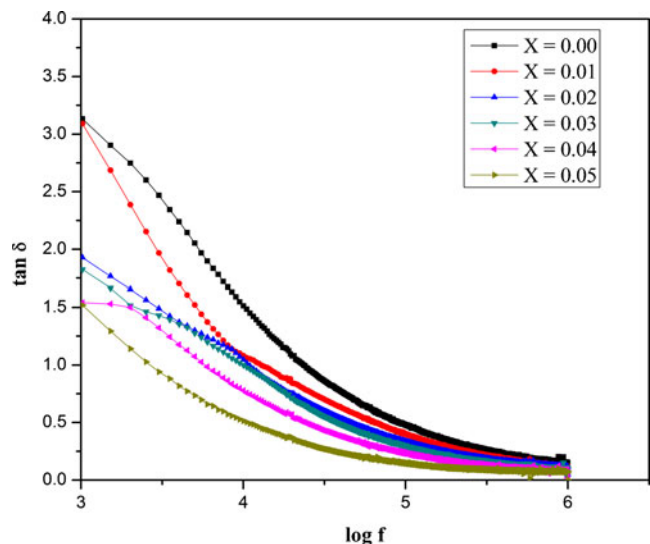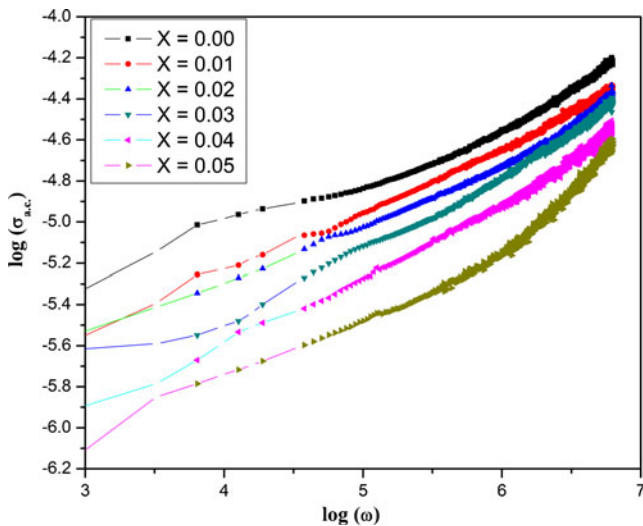$$M^*(\omega) = \frac{1}{\varepsilon^*(\omega)} = M'(\omega) + iM''(\omega), \quad (5)$$

The real (M') and imaginary (M'') parts of the complex electrical modulus are obtained from $\varepsilon'(\omega)$ and $\varepsilon''(\omega)$ values using the relation

$$M'(\omega) = \frac{\varepsilon'(\omega)}{\varepsilon'(\omega)^2 + \varepsilon''(\omega)^2} \quad \text{and} \quad M''(\omega) = \frac{\varepsilon''(\omega)}{\varepsilon'(\omega)^2 + \varepsilon''(\omega)^2}, \quad (6)$$

Based on Eq. (6), we have changed the form of presentation of the dielectric data from $\varepsilon'(\omega)$ and $\varepsilon''(\omega)$ to $M'(\omega)$ and $M''(\omega)$. As a convenient measure of the characteristic relaxation time one can choose the inverse of frequency of the maximum position, i.e. $(2\pi f_{max})^{-1}$. Thus we can determine the composition dependence of the characteristic relaxation time straightforwardly from Fig. 10. Data presented in this way exhibit a relaxation peak for $M''(\omega)$ that moves towards lower frequencies, which means that the relaxation
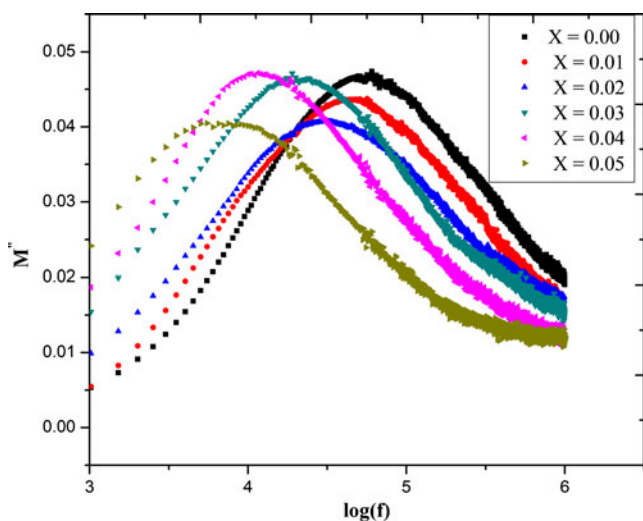
Fig. 7 Variation of dielectric constant (ε') as a function of logf for the MgAl$_{2-2x}$Y$_{2x}$O$_4$ (x=0.00–0.05) system

Fig. 8 Variation of dielectric loss tangent (tanδ) as a function of logf for the MgAl$_{2-2x}$Y$_{2x}$O$_4$ (x=0.00–0.05) system

Fig. 9 Variation of AC conductivity log ($\sigma_{a.c}$) as a function of logω for the $MgAl_{2-2x}Y_{2x}O_4$ (x=0.00–0.05) system

time for the $MgAl_{2-2x}Y_{2x}O_4$ system increases with increase in yttrium content. This has been explained on the basis of the fact that with increase in yttrium concentration there is reduction in crystallite size due to which the grain boundary volume increases, thereby increasing the number of dipoles in the grain boundary significantly. Due to which interaction among the dipoles within the grain boundary increases and hence the dipole relaxation becomes slower, reducing the relaxation frequency.

From the numerical fitting analysis of a suitably normalized M'' (ω), we calculated full width at half maximum (FWHM) for all the samples. The shape of the M'' curves in Fig. 10 for various yttrium compositions looks alike, but differs in their FWHM. The values of FWHM obtained for the present $MgAl_{2-2x}Y_{2x}O_4$ system lies in the range from

1.56 to 1.79. These values of FWHM are found to be higher than those reported, where relaxation present in the material is of Debye type [28]. Therefore nanocrystalline $MgAl_{2-2x}Y_{2x}O_4$ (0.00≤x≤0.05) system exhibits non Debye nature.

3.3 Electrical resistivity measurements

Resistivity (ρ) versus temperature curves for $MgAl_{2-2x}Y_{2x}O_4$ (0.00≤x≤0.05) system in the range 303–373 K is shown in Fig. 11. An initial decrease in the resistivity with the rise in temperature can be observed for all samples. This is attributed to the moisture sensitive nature of magnesium aluminate, due to which moisture and impurities like CO_2 are trapped in the samples [29]. However, when all the trapped impurities are removed at temperature approximately above 350 K the resistivity increases for all the investigated samples. This ambiguity indicates that sufficient energy is available to thermally activate that charge carrier, but the necessary activation energy has not been attained in the investigated temperature range [10].

The room temperature dc resistivity of $MgAl_{2-2x}Y_{2x}O_4$ series as a function of Y-concentration is shown in the inset Fig. 11. From which it is clear that the resistivity increases with increase in yttrium concentration. The observed increase in dc resistivity may be correlated to the jump length (L) of the charge carries between Al^{3+} and Al^{2+} ions on the octahedral B- site. The jump length (L) is determined from the relation [25]:

$$L = \frac{\sqrt{2}}{4}a,\tag{7}$$

where a is the lattice Parameter. The values of jump length L as a function of Y content (x) are tabulated in Table 1. This

Fig. 10 Compositional dependence of M'' versus log f for $MgAl_{2-2x}Y_{2x}O_4$ (x=0.00–0.05) system
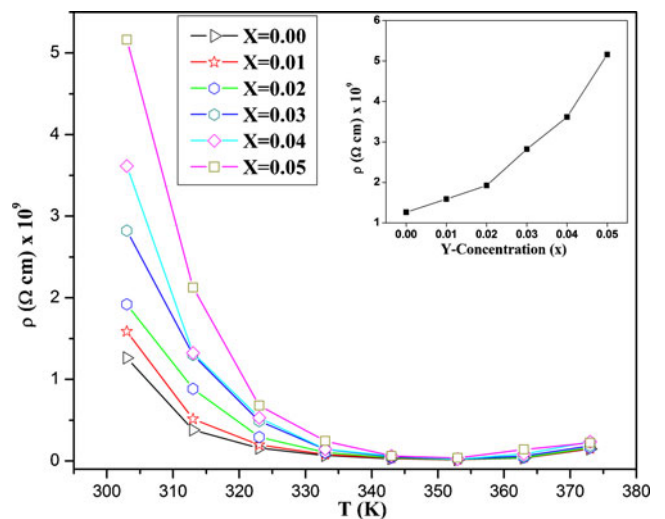
Fig. 11 Variation of resistivity (ρ) as a function of temperature in the range (303–373 K) for the $MgAl_{2-2x}Y_{2x}O_4$ (x=0.00–0.05) system. The inset shows room temperature resistivity of the samples

shows that L increases with increasing Y content. The observed increase in L with Y suggests that charge carriers require more energy to jump from one cationic site to other, which causes an increase in resistivity with increasing Y content.

4 Conclusion

The single phase compositions of $MgAl_{2-2x}Y_{2x}O_4$ ($0.00 \leq x \leq 0.05$) nanocrystalline ceramics were synthesized by chemical coprecipitation technique using ammonia as a precipitating agent. The lattice parameter and X-ray density increases with incorporation of Y, which is consistent with the differences in ionic radii of Al and Y. The observed decrease in both the molar concentration of aluminum and intensity of the absorption band (ν_2) with an increase in yttrium content (x) indicates the occupancy of Y^{3+} ions at octahedral B-sites. Electron microscopy studies reveal the polycrystalline nature of the samples. This study shows that loss tangent decreases and resistivity increases with the increase of yttrium concentration. The presented results can favor the use of these materials in electronics and telecommunication industry.

References

1. E.J.W. Verway, E.L. Heilmann, J. Chem. Phys. **15**, 174 (1947)
2. N.W. Grimes, Phys. Technol. **6**, 22 (1975)
3. C. Baudin, R. Martinez, P. Pena, J. Am. Ceram. Soc. **78**, 1857 (1995)
4. J. Zhang, J. Zhai, H. Jiang, X. Yao, J. Appl. Phys. **104**, 084102 (2008)
5. R.W. Siegel, J. Phys. Chem. Solids **55**, 1097 (1994)
6. M. Sugimoto, J. Am. Ceram. Soc. **82**, 269 (1999)
7. S. Kurien, Structural and electrical properties of certain nanocrystalline aluminates, Ph.D. Thesis, (Mahatma Gandhi University, Kottayam, India, 2005), http://mgutheses.in/page/?q=T%201354&search=siby+kurien&page=1&rad=sc#
8. M.J. Iqbal, S. Farooq, Mater. Sci. Eng. B **136**, 140 (2007)
9. M.J. Iqbal, B. Ismail, J. Alloys Compd. **472**, 434 (2009)
10. M.J. Iqbal, B. Kishwar, Mater. Res. Bull. **44**, 753 (2008)
11. M.J. Iqbal, B. Ismail, J. Alloys Compd. **504**, 440 (2010)
12. G. Stojanovic, V. Srdic, M. Maletin, Phys. Status Solidi A **205**, 2464 (2008)
13. M. Ishaque, M.U. Islam, M. Azhar Khan, I.Z. Rahman, A. Genson, S. Hampshire, Phys. B **1532** (2010)
14. J. Salmones, J.A. Galicia, M.A. Wang, G. Valenzuela, J. Mater. Sci. Lett. **19**, 1033 (2000)
15. B.D. Cullity, S.R. Stock, *Elements of X-Ray Diffraction*, 3rd edn. (Prentice Hall, USA, 2001)
16. N.H. Vasoya, V.K. Lakhani, P.U. Sharma, K.B. Modi, R. Kumar, H.H. Joshi, J. Phys. Condens. Matter **18**, 8063 (2006)
17. P. Tarte, Spectrochim. Acta **23A**, 2127 (1967)
18. A.B. Gadkari, T.J. Shinde, P.N. Vasambekar, Mater. Chem. Phys. **114**, 505 (2009)
19. S.K. Behera, P. Barpanda, S.K. Pratihar, S. Bhattacharyya, Mater. Lett. **58**, 1451 (2004)
20. P. Barpanda, S.K. Behera, P.K. Gupta, S.K. Pratihar, S. Bhattacharyya, J. Eur. Ceram. Soc. **26**, 2603 (2006)
21. N. Rezlescu, E. Rezlescu, Solid State Commun. **14**, 69 (1974)
22. K. Iwauchi, Jpn. J. Appl. Phys. **10**, 1520 (1971)
23. J.C. Maxwell, *A Treatise on Electricity and Magnetism*, 2nd edn. (Dover Publications, New York, 1954)
24. C.G. Koops, Phys. Rev. **83**, 121 (1951)
25. A.S. Fawzi, A.D. Sheikh, V.L. Mathe, J. Alloys Compd. **502**, 231 (2010)
26. I.G. Austin, N.F. Mott, Adv. Phys. **18**, 41 (1969)
27. J.H. Ambrus, C.T. Moyniham, P.B. Macedo, J. Phys. Chem. **76**, 3287 (1972)
28. A.H. Elsayed, A.M. Haffz, Egypt. J. Solids **28**, 53 (2005)
29. K. Ahn, B.W. Wessels, S. Sampath, Sensors Actuator B. Chem. **107**, 342 (2005)